Robust Control of a High Redundancy Actuator

Thomas Steffen, Roger Dixon, Roger Goodall, Argyrios Zolotas

Control Systems Group,
Department of Electronic and Electrical Engineering,
Loughborough University, Loughborough, LE11 3TU, UK,
http://www.lboro.ac.uk/departments/el/research/scg/
t.steffen, r.dixon, r.m.goodall, a.c.zolotas@lboro.ac.uk

Abstract: The High Redundancy Actuator project deals with the construction of an actuator using many redundant actuation elements. Whilst this promises a high degree of fault tolerance, the high number of components poses a unique challenge from a control perspective.
This paper shows how a simple robust controller can be used to control the system both in nominal state and after faults. To simplify the design task, the parameters of the system are tuned so that a number of internal states are decoupled from the input signal. If the decoupling is not exact, there may be small deviation from the nominal transfer function, especially when a fault has occurred. The robustness analysis ensures that the system performs well for all expected behaviour variations.

Keywords: high redundancy actuator, fault-tolerant control, fault accommodation, robust control, parameter uncertainties.

1. HIGH REDUNDANCY ACTUATION

High Redundancy Actuation (HRA) is a new approach to fault tolerant actuation, where an actuator comprises of a large number of actuation elements (see Figure 1). Faults in the individual elements can be accommodated without resulting in a failure of the complete actuator system.

The concept of the High Redundancy Actuation (HRA) is inspired by the human musculature. A muscle is composed of many individual muscle cells, each of which provides only a minute contribution to the force and the travel of the muscle. The aim of this project is to use the same principle of co-operation with existing actuation technology to provide intrinsic fault tolerance.

An important feature of the High Redundancy Actuator is that the actuator elements are connected both in parallel and in series. The reason is that the serial stacking of elements is the only configuration that can effectively deal with the lock-up of an element. A purely parallel configuration can deal well with loose elements, but a lock-up would affect all elements. Due to the series configuration, this fault only leads to a reduction of available travel.

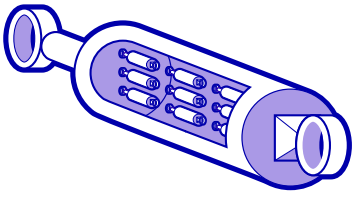

Figure 1. Configuration of a High Redundancy Actuator

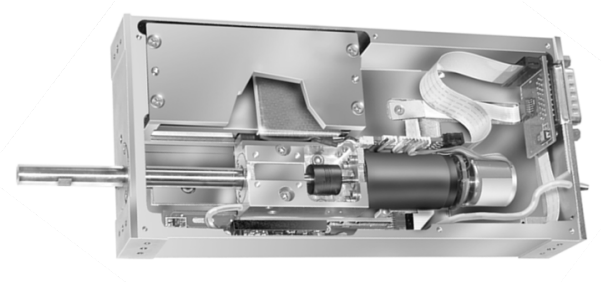

Figure 2. Electromagnetic actuator (photo by SMAC Inc.)

Modelling each mass individually leads to a high order dynamic model. For the envisioned number of elements (10x10 or more), the model may have hundreds of states, which is too complex for typical multi-variable control approaches (see Du et al., 2006, 2007). Thus the goal of this paper is to reduce the implementation complexity by using a simple robust controller. The controller has to be able to deal with modelling uncertainties and with behavioural changes caused by faults. A robust control strategy is used to avoid relying on adaptation or reconfiguration.

Section 2 is concerned with the modelling of the nominal system, followed by the treatment of faults and parameter tolerances in Section 3 and 4. The controller is designed in Section 5 and analysed for robustness in Section 6. Simulation results are discussed in Section 7, followed by a summary of further research avenues in Section 8.

2. NOMINAL MODEL

This paper is concerned with electromagnetic actuation, which is similar to a voice coil in operation. An example actuator is shown in Figure 2. An individual actuation

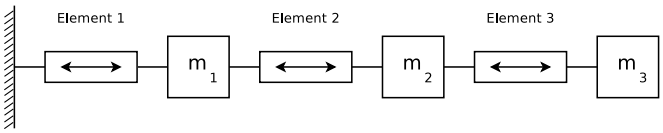

Figure 3. Three Actuation Elements in Series

element can be modelled as a spring-damper system, following Newton's second law of motion (see Davies et al. 2008 for full details):

$$m\ddot{x} = ki - d\dot{x} - rx \quad ,$$

where x is the position, m is the moving mass, k is the input coefficient, d is the damping factor, r is the elasticity of the spring, i is the current input and x is the position of the mass. Choosing x and $\dot{x}$ as states leads to the following state space model:

$$\frac{d}{dt}\begin{pmatrix}\dot{x}\\ x\end{pmatrix} = \begin{pmatrix}-\frac{d}{m} & -\frac{r}{m}\\ 1 & 0\end{pmatrix}\begin{pmatrix}\dot{x}\\ x\end{pmatrix} + \begin{pmatrix}\frac{k}{m}\\ 0\end{pmatrix} i \quad . \qquad (1)$$

To keep the analysis simple, this paper deals with a system of only three elements (see Figure 3). However, the methods used scale well, and they can be applied to higher order models as necessary.

The state space model of the fault-less SI-SO system of three actuation elements is

$$\frac{d}{dt}\mathbf{x} = \mathbf{A}(\mathbf{q})\mathbf{x} + \mathbf{B}(\mathbf{q})\mathbf{i}$$
$$\mathbf{y} = \mathbf{C}(\mathbf{q})\mathbf{x}$$

with

$$\mathbf{x} = (\,\dot{x}_1\ x_1\ \dot{x}_2\ x_2\ \dot{x}_3\ x_3\,)^T$$
$$\mathbf{q} = (m_1\, m_2\, m_3\, k_1\, k_2\, k_3\, d_1\, d_2\, d_3\, r_1\, r_2\, r_3)^T$$
$$\mathbf{A}(\mathbf{q}) = \begin{pmatrix} -\frac{d_1+d_2}{m_1} & -\frac{r_1+r_2}{m_1} & \frac{d_2}{m_1} & \frac{r_2}{m_1} & 0 & 0\\ 1 & 0 & 0 & 0 & 0 & 0\\ \frac{d_2}{m_2} & \frac{r_2}{m_2} & -\frac{d_2+d_3}{m_2} & -\frac{r_2+r_3}{m_2} & \frac{d_3}{m_2} & \frac{r_3}{m_2}\\ 0 & 0 & 1 & 0 & 0 & 0\\ 0 & 0 & \frac{d_3}{m_3} & \frac{r_3}{m_3} & -\frac{d_3}{m_3} & -\frac{r_3}{m_3}\\ 0 & 0 & 0 & 0 & 1 & 0 \end{pmatrix}$$
$$\mathbf{B}(\mathbf{q}) = \begin{pmatrix} \frac{k_1-k_2}{m_1} & 0 & \frac{k_2-k_3}{m_2} & 0 & \frac{k_3}{m_3} & 0 \end{pmatrix}^T$$
$$\mathbf{C}(\mathbf{q}) = (\,0\ 0\ 0\ 0\ 0\ 1\,) \quad ,$$

where $\mathbf{x}$ is the state, $\mathbf{i}$ the input, $\mathbf{y}$ the output, and $\mathbf{q}$ the parameter vector. The same model also applies if three groups of several parallel elements are used, for example in a 3x3 grid structure, as long as there are only three moving masses in the system.

For further analysis, this system will be modelled using a numeric transfer function, based on the following parameters $\mathbf{q}_0$:

$$m_1 = m_2 = 0.2\,\text{kg} \quad m_3 = 1\,\text{kg}$$
$$d_1 = 12\,\frac{\text{N}}{\text{m}} \quad d_2 = 11\frac{1}{3}\,\frac{\text{N}}{\text{m}} \quad d_3 = 10\,\frac{\text{N}}{\text{m}}$$

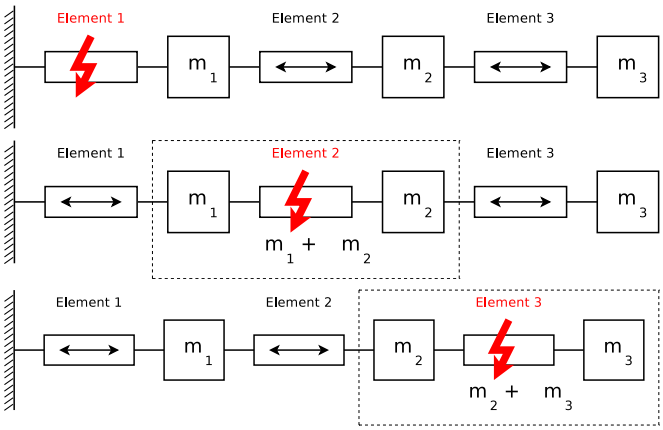

Figure 4. Faults in Elements 1, 2 and 3

$$r_1 = 1\frac{1}{5}\,\frac{\text{N}}{\text{m}} \quad r_2 = 1\frac{2}{15}\,\frac{\text{N}}{\text{m}} \quad r_3 = 1\,\frac{\text{N}}{\text{m}}$$
$$k_1 = 12\,\frac{\text{N}}{\text{A}} \quad k_2 = 11\frac{1}{3}\,\frac{\text{N}}{\text{A}} \quad k_3 = 10\,\frac{\text{N}}{\text{A}}$$

The resulting transfer function is

$$G_0(s,\mathbf{q}_0) = 10\frac{(s+179)(s+59.9)(s+0.1002)(s+0.1001)}{[(s+170)(s+59.9)(s+3.23)(s+0.1032)(s+0.1002)(s+0.1001)]}$$

which simplifies to

$$G_0(s,\mathbf{q}_0) = 10\frac{1}{(s+3.23)(s+0.103)} \quad , \qquad (2)$$

because the parameters have been carefully chosen to place the four input decoupling zeros over four of the six poles of the system (see Steffen et al., 2008 for further details). The four zeros are input decoupling zeros, which means that the four cancelled poles are uncontrollable, but not unobservable.

3. MODELLING FAULT CASES

Three fault cases are considered here: one for the blockage of each of the three actuation elements. In each fault case, the resulting system has only two moving masses (see Figure 4). The parameters differ slightly depending on which element has failed, but the structure is always the same. For example, the state space model after the blockage of the first element is:

$$\mathbf{x} = (\,\dot{x}_2\ x_2\ \dot{x}_3\ x_3\,)^T$$
$$\mathbf{A}_1(\mathbf{q}) = \begin{pmatrix} -\frac{d_2+d_3}{m_2} & -\frac{r_2+r_3}{m_2} & \frac{d_3}{m_2} & \frac{r_3}{m_2}\\ 1 & 0 & 0 & 0\\ \frac{d_3}{m_3} & \frac{r_3}{m_3} & -\frac{d_3}{m_3} & -\frac{r_3}{m_3}\\ 0 & 0 & 1 & 0 \end{pmatrix}$$
$$\mathbf{B}_1(\mathbf{q}) = \begin{pmatrix} \frac{k_2-k_3}{m_2} & 0 & \frac{k_3}{m_3} & 0 \end{pmatrix}^T$$
$$\mathbf{C}_1(\mathbf{q}) = (\,0\ 0\ 0\ 1\,) \quad .$$

The resulting transfer functions for the fault cases are

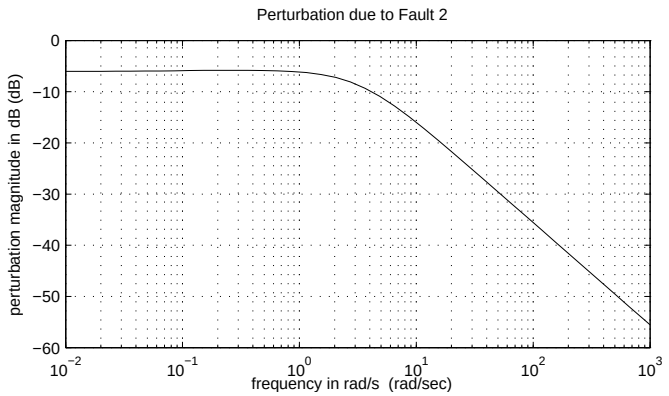

Figure 5. Perturbation $|\Delta_2(j\omega)|$ caused by Fault 2

$$G_1(s,\mathbf{q}_0)=10\frac{s+113}{s+112}\frac{1}{(s+4.98)(s+0.102)} \quad (3)$$

$$G_2(s,\mathbf{q}_0)=10\frac{1}{(s+4.90)(s+0.102)} \quad (4)$$

$$G_3(s,\mathbf{q}_0)=9.44\frac{s+120}{s+121}\frac{1}{(s+4.56)(s+0.102)}\,. \quad (5)$$

Compared to the nominal system, the main change is that the pole at 3.23 becomes faster by about 50 %. There is also a slight misalignment of a pole/zero pair around 120 in G_1 and G_2, and a minimal shift of the slowest pole. The amplification is reduced slightly in G_3, due to the increase in the weight of the load.

Because $G_2(s)$ has the simplest structure, it will be considered the reference case that is compared to the nominal system. The other transfer functions are then compared against $G_2(s)$. The multiplicative error introduced by Fault 2 compared to the nominal system is [1]

$$1-\Delta_2(s)=\frac{G_0(s)}{G_2(s)}=\frac{s+4.90}{s+3.23}\frac{s+0.102}{s+0.103}\,. \quad (6)$$

The amplitude of the frequency response $|\Delta_2(j\omega)|$ is shown in Figure 5, which reveals as a strong frequency dependence. The maximum is around -6 dB or 0.5 for low frequencies, and it falls off for frequencies above 5 rad/s.

The errors introduced by the other faults relative to G_2

$$1+\Delta_{1,2}(s)=\frac{G_1(s,\mathbf{q}_0)}{G_2(s,\mathbf{q}_0)}=\frac{s+113}{s+112}\frac{s+4.90}{s+4.98} \quad (7)$$

$$1+\Delta_{3,2}(s)=\frac{G_3(s,\mathbf{q}_0)}{G_2(s,\mathbf{q}_0)}=0.944\frac{s+120}{s+121}\frac{s+4.90}{s+4.56} \quad (8)$$

are small as expected from the transfer functions, satisfying the bounds

$$|\Delta_{1,2}(j\omega)|<0.017=\Delta_{1,2,max} \quad (9)$$

$$|\Delta_{3,2}(j\omega)|<0.070=\Delta_{3,2,max} \quad . \quad (10)$$

4. PARAMETER TOLERANCES

The given transfer functions only apply if all system parameters have nominal values. In practice this may not be the case, so the effect of parameter tolerances on the transfer function needs to be considered. An interval or tolerance band of 5 % is assumed around the nominal values:

$$q_i\in\left[\frac{1}{1.05}q_{0,i},1.05\,q_{0,i}\right] \quad .$$

The whole set of possible parameter vectors $\mathbf{q}$ is a multi-dimensional interval

$$\mathbf{Q}=\left[\frac{1}{1.05}q_{0,1},1.05\,q_{0,1}\right]\times\ldots\times\left[\frac{1}{1.05}q_{0,12},1.05\,q_{0,12}\right]\,.$$

To be consistent with the results of the previous sections, this structured perturbations needs to be converted into an unstructured multiplicative error of the open loop transfer function. This error $\Delta(s,\mathbf{q})$ is defined as

$$\Delta(s,\mathbf{q})=\frac{G_0(s,\mathbf{q}_0)-G_0(s,\mathbf{q})}{G_0(s,\mathbf{q})} \quad (11)$$

and bounded by

$$|\Delta(j\omega,\mathbf{q})|\le\Delta_{\mathbf{Q},\max} \quad ,$$

where $G_0(s,\mathbf{q}_0)$ and $G_0(s,\mathbf{q})$ are the nominal and actual transfer functions, and $\Delta_{\mathbf{q},max}$ is the maximal width of the tolerance band. Calculating $\Delta_{\mathbf{q},max}$ is a complex task, and an overview of possible approaches can be found in Chapters 8–10 in Ackermann, 2002. Two methods will be presented here.

The first method is an approximation, but it is both intuitive and fast. Each parameter is considered separately using a vector $\mathbf{q}_i$, which differs only in the component $q_{i,i}$ from $\mathbf{q}_0$. Each parameters generates a multiplicative error band $|\Delta(jw,\mathbf{q}_i)|$. These bands are then added up to estimate the combined error of parameter tolerances. The result is shown in Figure 6. While this result is very visual, it is only a first order approximation of the maximum error, because effects cause by the correlation of two parameters are neglected. The maximum error found this way is

$$\Delta_{\mathbf{Q},\max}=0.114 \quad . \quad (12)$$

This proves to be a conservative estimate, but further research is required to determine why.

The second method is to put a grid over the parameter space, and only consider points on the grid. Because of the small tolerances, it is sufficient to consider only the corners of $\mathbf{Q}$, which are defined by the two end-points of each tolerance interval (plus and minus 5 %). Since any combination may be relevant, 2^{12} parameter vectors need to be considered. With a modern computer, this set can be processed in a reasonable amount of time, and the resulting error graphs are shown Figure 7. The maximum error recorded is

$$\Delta_{\mathbf{Q},\max}=0.108 \quad . \quad (13)$$

Note that with both methods, the bound shows little variation with frequency. This has implications for the robust control design, because it is not possible to tune the sensitivity function to peak at a frequency with a low maximum error.

The same approach is applied to the fault case models, leading to nearly identical results.

[1] The definition of Δ used here is slightly unusual, but it leads to much simpler results during the analysis.

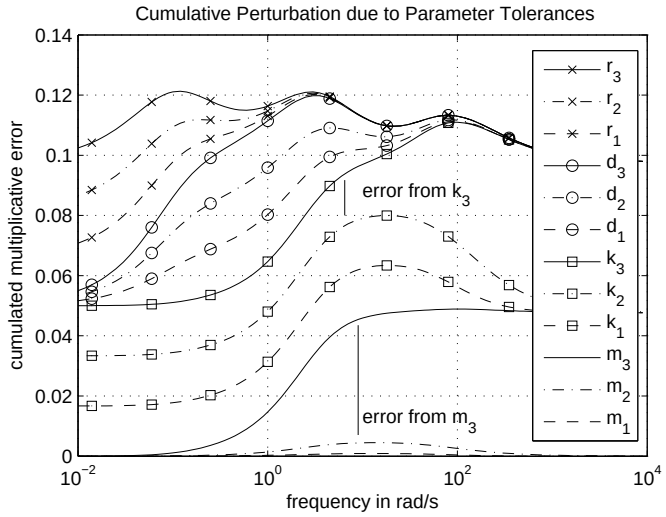

Figure 6. Cumulative error $\sum_i |\Delta(j\omega, \mathbf{q}_i)|$

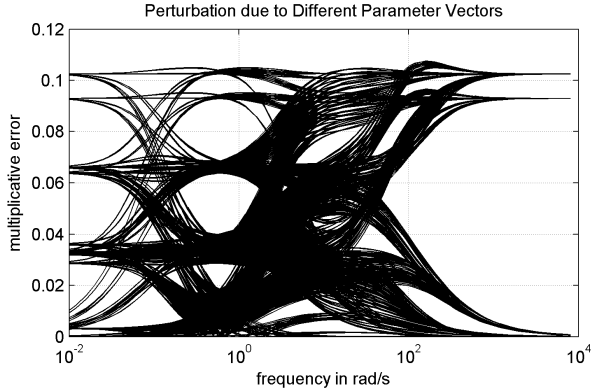

Figure 7. Error $|\Delta(j\omega, \mathbf{q})|$ for extreme choices of $\mathbf{q} \in \mathbf{Q}$

5. CONTROLLER DESIGN

The controller is designed using the nominal model G_0 for a fast 95 % settling time and minimal overshoot (see Steffen et al., 2007 for further details). A single input/single output proportional/integral controller with a phase advance compensator (SI-SO PID) is used. The transfer function of the controller is

$$G_C(s) = K_C \frac{s + 3.23}{s + 100} \frac{s + 0.1032}{s} \quad . \tag{14}$$

The slow zero is chosen to compensate the slowest pole of the system, and the phase advance block speeds up the next pole by a factor of 15. Using the root locus method (see Figure 8), the magnification is chosen at the branching point of the dominant pole pair to be $K_C = 240$. This results in a critically damped second order system behaviour. Note that this controller design is the result of an iterative process involving the robustness analysis in the next section.

This results in a open loop transfer function of

$$G_L(s) = \frac{625}{(s + 50)s} \tag{15}$$

and a closed loop transfer function of

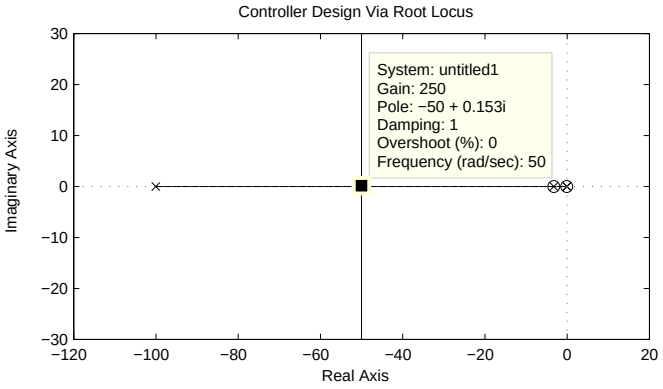

Figure 8. Root locus diagram for plant and controller

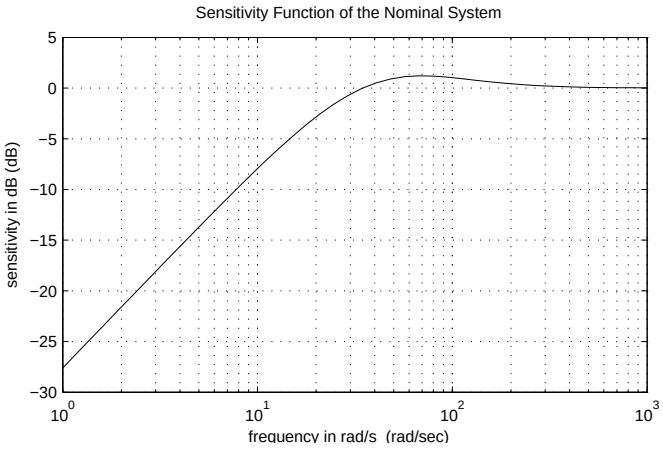

Figure 9. Sensitivity function $S(j\omega, \mathbf{q}_0)$ of the nominal loop

$$S(s) = \frac{1}{1 + G_L(s)} = \frac{s^2 + 50s}{(s + 25)(s + 25)} \tag{16}$$

from disturbance to output (identical to the sensitivity function) or

$$T(s) = 1 - S(s) = \frac{625}{(s + 25)(s + 25)} \tag{17}$$

from reference to output. Typical for a low pass system, the sensitivity function is small for low frequencies. It reaches a maximum of $S(j\omega) = 1.15$ or $+1.2\,\mathrm{dB}$ around $\omega = 68\,\mathrm{rad/s}$, and it remains around 1 for high frequencies (see Figure 9).

6. SENSITIVITY ANALYSIS

The analysis of the loop sensitivity is a valuable tool for understanding the robustness of a control loop. The sensitivity is a measure for how much a perturbation in the open loop transfer function affects the transfer function of the closed loop.

The multiplicative error of the closed loop behaviour $\tilde{T}(s, \mathbf{q})$ is

$$\frac{T(s)}{\tilde{T}(s, \mathbf{q})} - 1 = \frac{\frac{G_L(s)}{1+G_L(s)}}{\frac{\tilde{G}_L(s,\mathbf{q})}{1+\tilde{G}_L(s,\mathbf{q})}} - 1 = \frac{G_L(s) - \tilde{G}_L(s, \mathbf{q})}{(G_L(s) + 1) - \tilde{G}_L(s, \mathbf{q})}$$

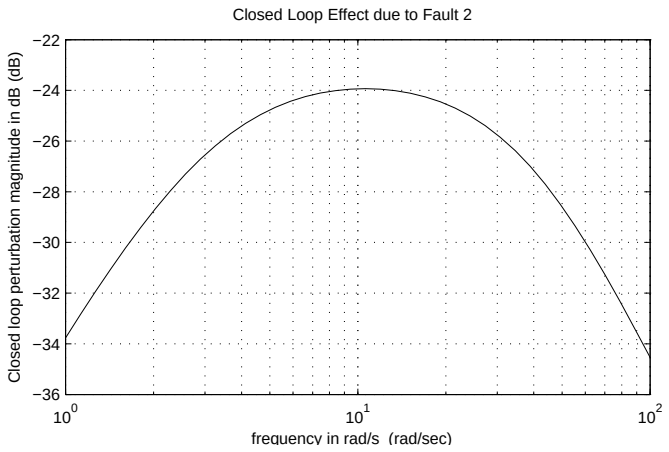

Figure 10. Closed loop perturbation $\Delta_2(j\omega)S(j\omega)$

$$= \frac{G_L(s) - \frac{G_L(s)}{1-\Delta(s,\mathbf{q})}}{(G_L(s)+1)\frac{G_L(s)}{1-\Delta(s,\mathbf{q})}} = \frac{-\Delta(s,\mathbf{q})}{G_L(s)+1} = -\Delta(s,\mathbf{q})S(s)\,,$$

where $G_L(s)$ and $T(s)$ represent the nominal open loop and closed loop behaviour, and $\tilde{G}_L(s,\mathbf{q})$ and $\tilde{T}(s,\mathbf{q})$ stand for the perturbed system subject to the multiplicative total perturbation $\Delta(s,\mathbf{q})$. The equation is generally applicable, and it covers parameter tolerances as well as faults. It highlights that the resulting closed loop perturbation can be reduced by lowering the sensitivity $S(s)$ or the perturbation $\Delta(s,\mathbf{q})$ for a given frequency. So the goal is keep the sensitivity function small in the low frequency range where perturbations have a significant influence.

The strongest error $\Delta_2(s)$ (caused by Fault 2) has a favourable frequency distribution (see Figure 5). The error drops off sharply beyond a frequency of $\omega = 5$. So the product $\Delta_2(j\omega)S(j\omega)$ remains relatively small, with a maximum of 0.06 or $-24\,\mathrm{dB}$ around $10\,\mathrm{rad/s}$ (see Figure 10). This separation is a direct result of the phase advance compensator, because it moves the rise of the sensitivity function to a higher frequency range.

The other two classes of errors (caused by parameter tolerances and the differences between the fault cases) affect a wide frequency range, so they reach into the region with high sensitivity. The overall effect is still limited, because of the small absolute size of the error. This is shown in Figure 11 for the parameter tolerances, and the effect of the differences between the fault cases is even smaller.

All errors are listed in Table 1. Since the errors are reasonably small, it can be assumed that they interact linearly. [2] So the maximum upper bounds can be added up.

The combined effect of all perturbations is just over 25 % or one quarter of the closed loop transfer function. Due to the shape of the sensitivity function, these changes are limited to the higher frequency range, while low frequencies and DC signals are unaffected. This means

[2] In the strict sense, this is only correct for the open loop perturbations, and only if they are expressed in a logarithmic scale (dB). However, for this application an approximation of the effect is sufficient.

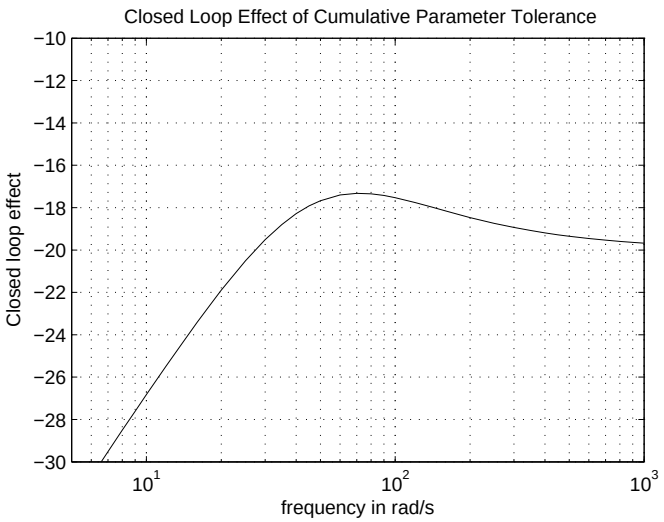

Figure 11. Effect of parameter perturbations on the system

Table 1. Summary of errors

Cause	Symbol	Open loop	Closed loop
Fault 2	Δ_2	$< 40\,\%$	$< 7\,\%$
Fault differences	$\Delta_{3,2}/\Delta_{1,2}$	$< 7\,\%$	$< 8\,\%$
Param. tolerances	Δ_0	$< 11\,\%$	$< 12\,\%$
Total perturbation			$<\approx 27\,\%$

that most aspects of the closed loop behaviour (such as bandwidth and resonance) change very little.

There is no easy way to assess the maximum overshoot based on these frequency domain results. For the dominant pole pair, the original damping is critical with $\zeta = 1$, and even a reduction to $\zeta = 0.7$ would not lead to excessive overshoot [Hu et al., 1996]. However, the dominant pole pair is not the only relevant influence in this case, because a number of slow pole-zero pairs have a significant influence on the system behaviour. So the overshoot has to be studied in the time domain.

7. SIMULATION RESULTS

The step response of the nominal system in comparison with the three fault cases is shown in Figure 12. As predicted in the sensitivity analysis, the faults have only a small influence on the behaviour of the system. There is no sign of overshoot, and the settling time is only slightly longer than in the nominal case.

There is however as small set-point deviation (less than 5 %), that remains present for quite a while. This is caused by the incomplete cancellation of the pole at -4.9 (instead of -3.2). In the frequency domain, the effect of this pole was quantified to be less than $-24\,\mathrm{dB}$, which corresponds well with the 5 % seen in the time domain. If this deviation is too much for a given application, further efforts can be made in the frequency domain to reduce the sensitivity to this pole position.

The influence of parameter tolerances is determined by selecting a high number of extreme parameter constellations at random. The results are shown in Figure 13, with an enlargement of the steady state region in Figure 14. There

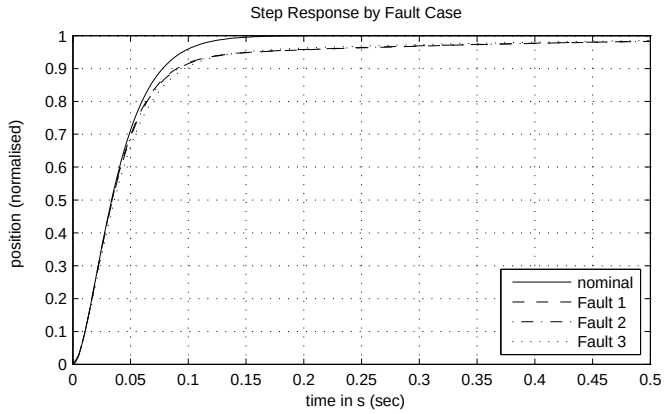

Figure 12. Step response with faults

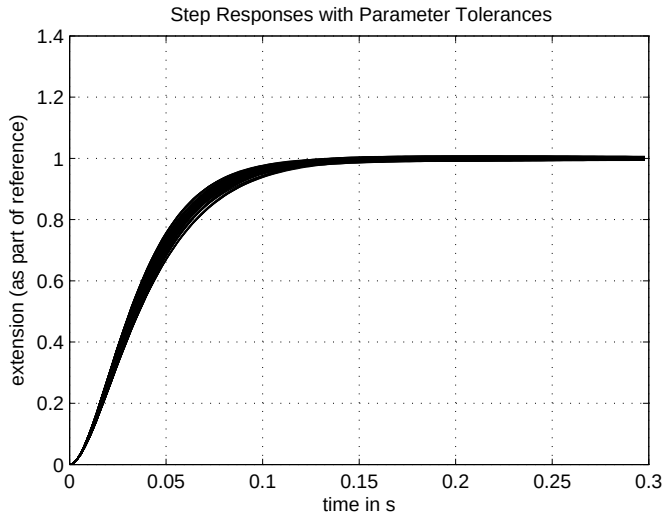

Figure 13. Step response with parameter tolerances

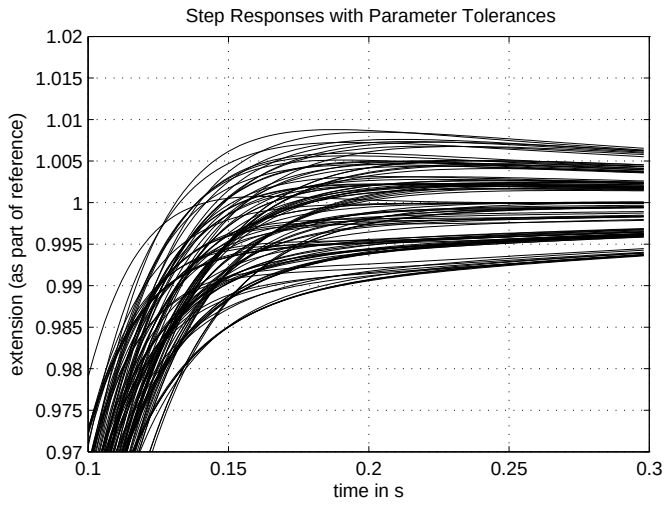

Figure 14. Step response with parameter tolerances

is no oscillation, but a small amount of overshoot (less than 1 %) is caused by incomplete pole-zero cancellations.

8. CONCLUSIONS AND FURTHER RESEARCH

The method demonstrated here can be used to prove the stability of a given controller for all relevant fault cases. A simple PI controller with a phase advance compensator was found sufficient to satisfy the control problem in all considered cases. For more complicated systems, it would also be possible to use a higher order controller, or to add a pre-filter to the control loop.

Further research will extend the results presented here to make them more generally applicable. It is important to derive generic results for arbitrary numbers of elements, even if these results may be more conservative than can be found for a specific case. Another aim is to derive algebraic results that are independent of the parameters values. Finally, the influence of different controllers and different actuator configurations has to be assessed.

9. ACKNOWLEDGEMENTS

This project is a cooperation of the Control Systems group at Loughborough University, the Systems Engineering and Innovation Centre (SEIC), and the actuator supplier SMAC Europe limited. The project is funded by the Engineering and Physical Sciences Research Council (EPSRC) of the UK under reference EP/D078350/1.

REFERENCES

JÃŒrgen Ackermann. *Robust control: the parameter space approach*. Springer, Berlin, 2002. ISBN 1852335149.

J. Davies, T. Steffen, R. Dixon, R. M. Goodall, A. C. Zolotas, and J. Pearson. Modelling of high redundancy actuation utilising multiple moving coil actuators. In *Proceedings of the IFAC World Congress 2008*, Jul 6-11 2008. submitted.

X. Du, R. Dixon, R. M. Goodall, and A. C. Zolotas. Assessment of strategies for control of high redundancy actuators. In *Proceedings of the ACTUATOR 2006*, 2006.

X. Du, R. Dixon, R. M. Goodall, and A. C. Zolotas. Lqg control for a high redundancy actuator. In *Proceedings of the 2007 IEEE/ASME International Conference on Advanced Intelligent Mechatronics*, 2007.

J. Hu, H. Unbehauen, and C. Bohn. A practical approach to selecting weighting functions for h infinity control and its application to a pilot plant. In *Proceedings of the UKACC International Conference on Control '96*, volume 2, pages 998–1003, 2-5 Sept. 1996 1996. ISBN 0-85296-668-7.

T. Steffen, R. Dixon, R. M. Goodall, and A. C. Zolotas. Requirements analysis for high redundancy actuation. Technical Report CSG-HRA-2007-TR-4, 2007.

T. Steffen, R. Dixon, R. M. Goodall, and A. Zolotas. Multi-variable control of a high redundancy actuator. In *Actuator 2008 – International Conference and Exhibition on New Actuators and Drive Systems – Conference Proceedings*, pages 473—476. HVG, 2008. ISBN 3-933339-10-3.